Nucleic Acids Research, 2001, Vol. 29, No. 19 **4089–4096**

Comparison between CUUG and UUCG tetraloops: thermodynamic stability and structural features analyzed by UV absorption and vibrational spectroscopy

Vladimir Baumruk[1,2], Catherine Gouyette[3], Tam Huynh-Dinh[3], Jian-Sheng Sun[4] and Mahmoud Ghomi[2,*]

[1]Institute of Physics, Charles University, Ke Karlovu 5, 121 16 Prague 2, Czech Republic, [2]Laboratoire de Physicochimie Biomoléculaire et Cellulaire, UMR CNRS 7033, Université Pierre et Marie Curie, Case 138, 4 Place Jussieu, 75252 Paris Cedex 05, France, [3]Unité de Chimie Organique, URA CNRS 2128, Institut Pasteur, 28 rue du Docteur Roux, 75724 Paris Cedex 15, France and [4]Laboratoire de Biophysique, UMR 8646 CNRS, Muséum National d'Histoire Naturelle, INSERM U201, 43 rue Cuvier, 75231 Paris Cedex 05, France

Received March 30, 2001; Revised and Accepted August 7, 2001

ABSTRACT

CUUG loop is one of the most frequently occurring tetraloops in bacterial 16S rRNA. This tetraloop has a high thermodynamic stability as proved by previous UV absorption and NMR experiments. Here, we present our results concerning the thermodynamic and structural features of the 10mer 5′-r(GCG-CUUG-CGC)-3′, forming a highly stable CUUG tetraloop hairpin in aqueous solution, by means of several optical techniques (UV and FT-IR absorption, Raman scattering). UV melting profile of this decamer provides a high melting temperature (60.7°C). A set of Raman spectra recorded at different temperatures allowed us to analyze the order-to-disorder (hairpin-to-random coil) transition. Assignment of vibrational markers led us to confirm the particular nucleoside conformation, and to get information on the base stacking and base pairing in the hairpin structure. Moreover, comparison of the data obtained from two highly stable CUUG and UUCG tetraloops containing the same nucleotides but in a different order permitted an overall discussion of their structural features on the basis of Raman marker evidences.

INTRODUCTION

UNCG, GNRA and CUUG sequences (where N = U, A, C, G; and R = G, A) form very stable and conserved tetraloops that play an important role in structural stability and biological function of 16S rRNA (1–3). Three-dimensional structures of a few of these tetraloops have been determined by high resolution NMR spectroscopy, i.e. UUCG (4,5), UACG (6,7), GAAA (8), GCAA (8), GAGA (8,9) and CUUG (10). Although all these hairpins have an A-form stem, their loop turns differ completely from one family to another (reviewed in 10,11).

The CUUG tetraloop is a highly conserved one, found between positions 83–87 of bacterial 16S rRNA (2). The closing base pair of this tetraloop is frequently a G-C rather than a C-G one, as in UNCG and GNRA tetraloops. Conformational angles of the CUUG tetraloop are available from the NMR data related to the 12mer 5′-r(GGCG-CUUG-CGUC)-3′ (10) (atomic cartesian coordinates allowing to calculate the conformational angles are accessible in a file deposited on the PubMed site, MMDB Id: 3979, PDB Id: 1RNG). They can reveal that all the glycosidic angles are in the *anti* range, and the four CUUG loop nucleotides adopt almost C2′-*endo* type sugar puckers. More precisely, the pseudorotation P angles (12) of the loop sugars are found in the 129–154° range that corresponds to the C1′-*exo* to C2′-*endo* puckering. The conformational features of the CUUG tetraloop can be more strongly stressed through their comparison with those of the UUCG tetraloop consisting of the same residues but in a different order. In contrast to UUCG, CUUG is stabilized by a standard Watson–Crick C-G base pair formed between the first and the last loop nucleotide. The second U in the UUCG tetraloop points out, whereas in the CUUG loop it is folded into the minor groove and interacts with the loop C-G base pair and the stem G-C (closing) base pair (10). Moreover, the third C in the UUCG is 3′-stacked, while U in the same position in the CUUG is 5′-stacked with the loop and stem bases (Fig. 1). The above-mentioned differences as well as those in the α/ζ and γ torsion angles lead to formation of two very distinct intramolecular hydrogen bond networks stabilizing these two tetraloops (10,11).

Vibrational spectroscopy, and particularly Raman spectroscopy, has shown its ability to probe structural features of nucleic acids (reveiwed in 13–16) by means of (i) nucleoside conformation markers as indicators of sugar pucker and glycosidic torsion and (ii) phosphate-backbone conformation markers as indicators of helical conformations. Recent

*To whom correspondence should be addressed. Tel: +33 1 44277555; Fax: +33 1 44277560; Email: ghomi@lpbc.jussieu.fr

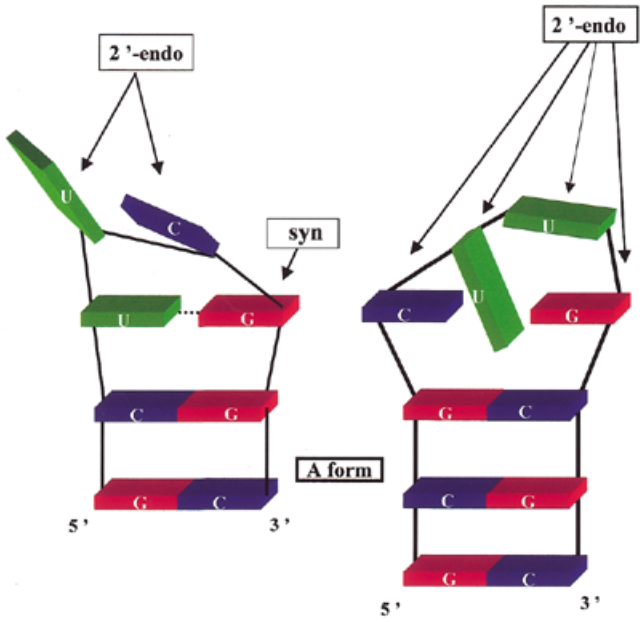

Figure 1. Schematic relative positions of the base residues in UUCG (left) and CUUG (right) hairpins as predicted from NMR data (10,11). Stems form intramolecular A-form double helices. All the nucleotides are in the C3′-*endo/anti* conformation unless otherwise indicated.

comparative study of different genomic DNAs has convincingly demonstrated sequence-related structural sensitivity of Raman spectroscopy (17) and its capability to distinguish genomic DNAs by means of their characteristic Raman signatures. We have already exploited this important feature of Raman spectroscopy to study the effect of the non-conservative residue (N) in the UNCG family tetraloops on their structural features and stability through the 8mers 5′-r(GC-UNCG-GC)-3′ (where N = U, A, C, G) (7,18,19). Raman data have been completed by those from UV and FT-IR absorption. A similar approach was applied to a number of GNRA tetraloops through the analysis of the 10mers 5′-r(CGC-GNRA-GCG)-3′ (where N = A, C, U; and R = A, G) sequences (19,20). Raman spectra of the above-mentioned sequences collected as a function of temperature, provided us with the possibility of analysing the order-to-disorder transition of these hairpins.

In the present work, we describe how Raman spectroscopy can be used as a probe to emphasize the sequence-related structural differences between CUUG and UUCG tetraloop hairpins. A detailed comparative study of Raman signatures of the two RNA tetraloops has been facilitated by improvement of the spectrometer performance and the measurement protocol. The new set of experimental data reported here on the CUUG tetraloop completes those reported previously on UV absorption (21,22) and NMR spectroscopy (10).

MATERIALS AND METHODS

Chemical synthesis

The decamer 5′-r(GCG-CUUG-CGC)-3′ was synthesized at the Institut Pasteur in Paris, following the procedure described previously (7). Approximately 5 mg of purified lyophilized sample was obtained (containing 1 Na^+ per phosphate group). Hereafter this sequence is referred to as CUUG decamer or CUUG hairpin. The main difference between the presently studied 10mer and the 12mer 5′-r(GGCG-CUUG-CGUC)-3′, previously studied by means of NMR spectroscopy (10), is the lack of one G and one U on the 5′- and 3′-sides of the central CUUG motif, respectively. The choice of a shorter oligonucleotide sequence in this work allowed us to avoid a possible G-U base pair formation in the stem of hairpin, and to equilibrate the Raman signal originating from the stem (six residues) and loop (four residues).

Sample preparation

All samples used in optical spectroscopic experiments are obtained by dissolving the CUUG decamer in a phosphate buffer. To prepare a stock solution of the phosphate buffer, 83.4 mg KH_2PO_4, 54.8 mg Na_2HPO_4 and 1 mg EDTA have been dissolved in 100 ml milipore water. This preparation led to a neutral solution (pH 6.8) containing 10 mM monovalent cations (Na^+ and K^+) and 1 mM EDTA. Then, a stock solution of nucleic acid has been prepared by dissolving 1.4 mg of oligomer in 50 µl of the phosphate buffer, leading to a decamer molar concentration of ~9 mM. No additional salt has been added to this solution. The samples used for Raman and IR spectroscopy have been directly taken from the stock solution ($C_{oligomer}$ = 9 mM). For UV absorption melting profiles, the stock solution was further diluted in additional phosphate buffer to final concentrations of 0.4 mM, 100 and 10 µM oligomer, respectively.

UV absorption, Raman and IR spectroscopy

UV absorption melting profiles at 260 nm were obtained using a UVIKON 940 spectrophotometer with a multi-sample holder connected to a circulating water bath with thermal programmer (NetLab). Cuvettes with 1 mm or 1 cm optical path length, containing oligonucleotide samples were rapidly heated to >85°C and then slowly cooled down during the melting experiment with the cooling rate 0.5°C/min. Reversible melting profiles were obtained.

Raman spectra were excited with the 488 nm line of an argon laser (Stabilite model 2017-04S, Spectra Physics) using ~150 mW of radiant power at the sample. The spectra were collected on a Jobin-Yvon T64000 spectrograph in a single mono configuration with a 1200 grooves/mm holographic grating and a holographic notch filter. The spectrograph is equipped with a liquid nitrogen cooled CCD detection system (Spectrum One, Jobin-Yvon) based on a Tektronix CCD chip of 2000 × 800 pixels. The effective spectral slit width was set to ~5 cm^{-1}. Spectra were averaged from 120 exposures of 10 s each to produce the traces shown below. For each temperature, the buffer spectrum was also collected and used to compensate the solution spectrum for contribution of the solvent. Raman frequencies of well-resolved bands are accurate to within ±0.2 cm^{-1}. To exclude all possible drifts of the wavenumber scale during collection of a set of Raman spectra at different temperatures and to keep it as stable as possible over a long period of time, a calibration spectrum of a neon lamp was recorded before each sample spectrum. Typically 24 calibration lines were employed to calibrate studied spectral region ~1280 cm^{-1} broad. Using this approach one can monitor even small shifts of peak maxima (<1 cm^{-1}) due to temperature change with a high degree of confidence. Detailed description of a calibration

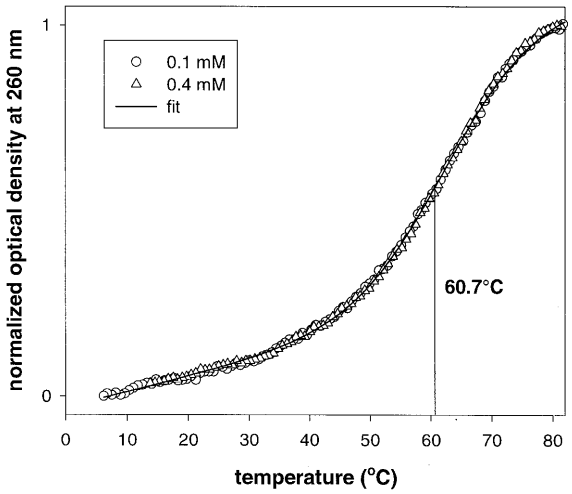

Figure 2. UV absorption melting profile of the 5′-r(GCG-CUUG-CGC)-3′ loop hairpin in aqueous solution at 0.4 mM and 100 μM concentrations. Basic thermodynamic parameters of the CUUG hairpin have been estimated with a simple two-state thermodynamic model (25): T_m = 333.7 K (60.7°C, shown by a vertical line), ΔH^0 = –28.1 kcal/mol and ΔS^0 = –84.0 cal/mol/K.

procedure will be given elsewhere. Spectral intensities were normalized to the water-bending band at ~1645 cm^{-1} using a subtraction coefficient of the buffer spectrum as a normalization parameter. The phosphodioxy stretching band (observed at ~1100 and ~1092 cm^{-1} for RNAs and DNAs, respectively) that is usually used for normalization of DNA spectra (23) cannot be employed because both its intensity and band shape are not invariant to the temperature range of interest.

Samples were placed in a microcell of 10 μm inner volume. Raman spectra were collected at ~5°C intervals in the range 3–80°C on samples thermostated to within ±0.1°C of the temperature indicated. The temperature gradient across the cell is <0.5°C. Reversibility of a structural transition (hairpin-to-disordered structure) was always checked after each heating cycle. Raman spectra taken at 20°C before and after heating procedure were virtually identical. A typical data set consists of 15 spectra that were analyzed to create temperature-dependent profiles of selected Raman bands.

In order to compare the intensities from the CUUG and UUCG hairpins, we have again recorded the Raman spectra from the 8mer 5′-(GC-UUCG-CG)-3′ using the Raman setup described above. The comparison between the new spectra for the UUCG hairpin and those published previously (7), clearly shows that the new Raman setup presents more resolved spectra without changing their general features (especially the wavenumbers of the main Raman marker bands). Thus, the new spectra of the UUCG hairpin are compared in this report with those obtained from the CUUG hairpin.

Infrared spectra were recorded at room temperature with a Nicolet Magna 860 FT-IR spectrometer using a standard source, a CsI beamsplitter and a DTGS detector. Usually 100 scans were collected with 4 cm^{-1} spectral resolution and a Happ-Genzel apodization function. Samples were placed in a demountable cell (Graseby Specac) consisting of a pair of CaF_2 windows and 12 μm Mylar spacer. Spectral contribution of a buffer in carbonyl stretching region was corrected following the standard algorithm (24).

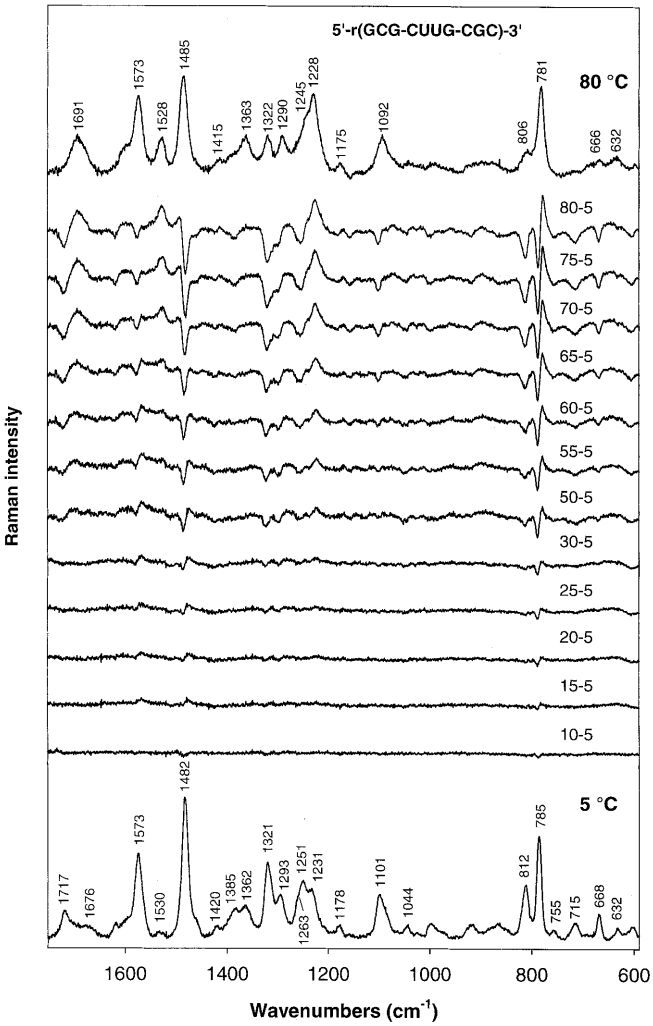

Figure 3. Aqueous solution Raman spectra (λ_{exc} = 488 nm) of 5′-r(GCG-CUUG-CGC)-3′ at 5°C (bottom trace) and 80°C (top trace) in the 1750–590 cm^{-1} spectral region. Intermediate traces represent the difference spectra calculated using the indicated higher temperature spectrum as minuend and the 5°C spectrum as subtrahend.

All spectral data were treated using a GRAMS/32 software (Galactic Industries). Owing to a good signal/noise ratio and accuracy of wavenumber scale, it was possible to follow recent trend (24) and present specific Raman band intensity changes or wavenumber shifts with temperature by means of difference spectra.

RESULTS AND DISCUSSION

Thermodynamic stability of CUUG tetraloop hairpin

UV absorption melting profile. Melting profiles obtained at 0.4 mM and 100 μM concentrations show a unimolar, progressive, reversible and concentration independent hairpin-to-random chain transition (Fig. 2). Two previous papers (21,22) have already reported high thermodynamic stability of the CUUG tetraloop in the 12mer 5′-r(GGAG-CUUG-CUCC)-3′. One of these papers (21) confirms the intramolecular hairpin as the dominant species, but according to the other (22) the

Table 1. Wavenumbers (cm^{-1}) and tentative assignments of Raman bands of the CUUG and UUCG hairpins recorded at 20°C

CUUG hairpin[a]	UUCG hairpin[b]	Assignment
1717 (m)	1710 (sh)	G C=O bond stretch; stem
1676 (w)	1689 (m)	U and G C=O bond stretch; loop and stem
1617 (sh)	1617 (sh)	U ring; loop
1600 (sh)	1600 (m)	C ring; stem and loop
1573 (vs)	1574 (vs)	G ring; stem and loop
1530 (w)	1530 (w)	C ring; stem and loop
1482 (vs)	1481 (vs)	G ring; stem and loop
1461 (sh)		U and C; loop and stem
1420 (w)	1418 (m)	r(G); stem and loop
	1403 (m)	r(U); loop
1385 (m)	1382 (m)	r(G); stem and loop; ordered structure
1362 (m)	1360 (m)	r(G); stem and loop; ordered and disordered structures
	1346 (sh)	r(G); stem and loop
1321 (s)	1321 (vs)	r(G); 3′-*endo/syn*; loop and r(G); 3′-*endo/anti*; stem
1313 (sh)		r(G); 2′-*endo/anti*; loop
1293 (m)	1294 (m)	r(C); 3′-*endo/anti*; stem and loop
1263 (sh)	1261 (sh)	r(C); 2′-*endo/anti*; loop
1251 (s)	1249 (sh)	r(C); 3′-*endo/anti*; loop and stem
1231 (s)	1234 (vs)	r(U); loop
1207 (sh)	1213 (sh)	
1178 (w)	1183 (w)	r(G); stem and loop
1101 (m)	1099 (m)	PO_2^- symmetric stretch
1044 (w)	1044 (w)	backbone, ribose
999 (w)	999 (w)	backbone
973 (w, sh)	973 (w, sh)	backbone
	925 (w)	backbone
918 (w, br)	916 (sh)	backbone
	880 (w, br)	backbone
870 (w, br)	868 (w, br))	phosphate-backbone
	848 (w, br)	phosphate-backbone
812 (s)	810 (s)	O-P-O symmetric stretch (A marker)
785 (vs)	785 (vs)	r(C) breathing mode; stem and loop; r(U) breathing mode; loop
715 (w)	715 (w)	backbone (A marker)
668 (w)	671 (w)	r(G); 3′-*endo/anti*; loop and stem
	638 (w)	r(G); 3′-*endo/syn*; loop
632 (w)	632 (w)	r(U); loop

vs, very strong; s, strong; m, medium; w, weak; vw, very weak; br, broad; sh, shoulder.
[a]As formed in aqueous solutions of 5′-r[GCG-CUUG-CGC]-3′ decamer (Fig. 6A).
[b]As formed in aqueous solutions of 5′-r[GC-UUCG-GC]-3′ octamer (Fig. 6A).

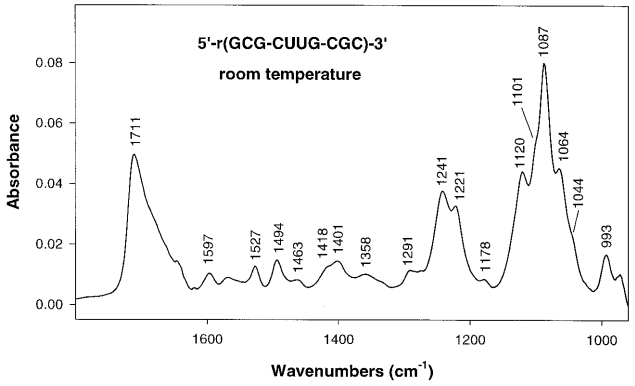

Figure 4. FT-IR spectrum of the 5′-r(GCG-CUUG-CGC)-3′ hairpin recorded at room temperature in the 1800–980 spectral region.

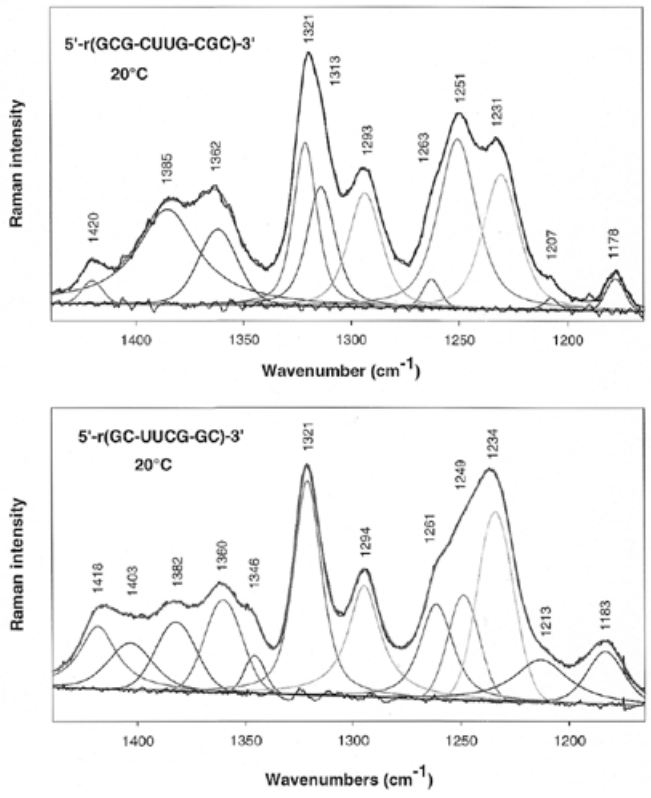

Figure 5. Tentative band decomposition of the Raman spectra (λ_{exc} = 488 nm) of 5′-r(GCG-CUUG-CGC)-3′ (top) and 5′-r(GC-UUCG-CG)-3′ (bottom) hairpins recorded at 20°C in the 1440–1140 cm^{-1} region.

possibility of duplex formation cannot be completely excluded at high salt concentration (1 M NaCl). In the present work the salt concentration was always well below this limit and no evidence of duplex formation has been found (see sample preparation).

Using a simple two-state thermodynamic model (25), basic thermodynamic parameters of the CUUG hairpin have been estimated as follows: T_m = 333.7 K (60.7°C), ΔH^0 = –28.1 kcal/mol and ΔS^0 = –84.0 cal/mol/K.

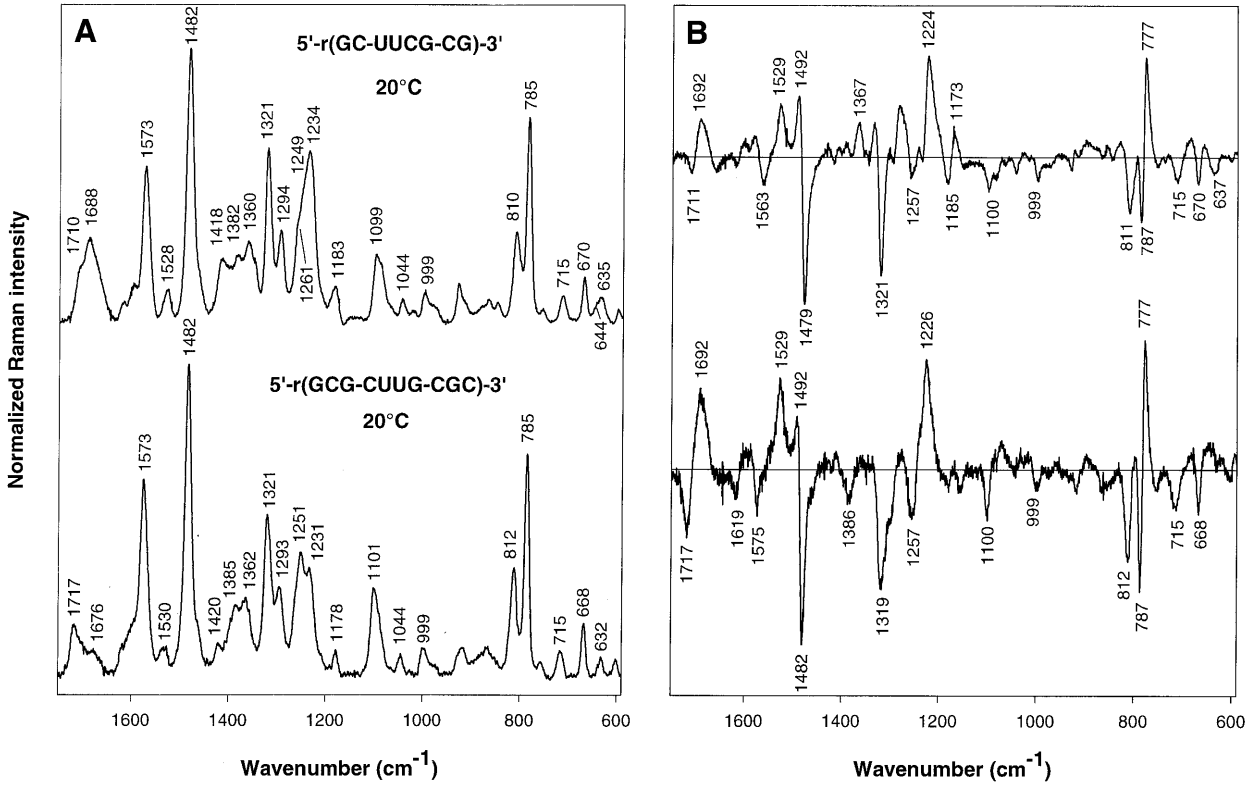

Figure 6. (**A**) Raman spectra (λ_{exc} = 488 nm) of 5′-r(GC-UUCG-CG)-3′ (top) and 5′-r(GCG-CUUG-CGC)-3′ (bottom) hairpins recorded at 20°C in the 1730–600 spectral region. After spectral treatment of both hairpins (solvent and background subtraction), relative Raman spectra of the CUUG and UCCG hairpins have been compared by means of the band at ~1100 cm^{-1} (corresponding to PO_2^- symmetric stretching mode). As the octamer (UUCG hairpin) and decamer (CUUG hairpin) sequences possess seven and eight phosphate groups, respectively, the octamer spectrum intensity has been multiplied by a correction factor equal to 0.78 (= 7/9). (**B**) Corresponding difference spectra computed using the 20°C spectrum as subtrahend and the 80°C temperature spectrum as minuend.

Raman and FT-IR spectra. Raman spectra (1750–590 cm^{-1}) of the CUUG hairpin loop at 5°C and of a fully melted strand at 80°C are shown in Figure 3 as the bottom and top traces, respectively. Other traces there present difference spectra at intervals of ~5°C between the indicated intermediate temperature (minuend) and 5°C (subtrahend). The difference spectra illustrate that although the most pronounced changes occur between 55 and 70°C, the Raman signatures of the CUUG tetraloop hairpin are sensitive to temperature through the whole studied range 5–80°C.

The wavenumbers of the prominent Raman bands observed at 20°C (and therefore corresponding to the hairpin structure) together with their tentative assignments are summarized in Table 1.

First of all, a considerable downshift of the 1717 cm^{-1} Raman band (observed also as a strong band at 1711 cm^{-1} in FT-IR spectra) to 1690 cm^{-1} should be pointed out. A negative band increasing with temperature is clearly seen in the difference Raman spectra (Fig. 3). This band is mainly assigned to the stretching vibrations of carbonyls involved in the interbase hydrogen bonds. The same effect has been observed for all UNCG (7,18) and GNRA (19,20) hairpins studied earlier by Raman spectroscopy and can thus be considered as a Raman fingerprint of interbase H-bond breakdown upon increasing temperature.

As can be seen in Figure 3, the Raman band at 1385 cm^{-1} (attributed to the rG residue) disappears with increasing temperature. This effect is also an indicator of the order-to-disorder transition of the hairpin. It should be pointed out that this band was always present in all of the ordered conformers (hairpins) that we have studied up to now (7,18–20), and the transition towards a disordered chain (induced by temperature increase) has led to a considerable decrease of its intensity. In contrast, the Raman band at 1360 cm^{-1} is always present either in ordered or in disordered chains and even in a free rG or in 5′-rGMP (spectra not shown). We cannot yet confirm whether the presence of the 1385 cm^{-1} Raman band is due to the interbase H-bonding or to the base stacking which are obviously the main structural features of an ordered RNA chain.

Raman hypochromism in nucleic acids, i.e. change in the Raman intensity owing to the stacking of base residues, has been recognized since the earliest works devoted to application of Raman spectroscopy to structural study of nucleic acids (14,15,26). This effect is actually considered as a measure of the loss of base stacking with increasing temperature, and can be particularly stressed here (Fig. 3, appearing as negative bands in the difference Raman spectra) for the rG modes at 1573, 1482, 1385 and 1321 cm^{-1}, for the rC modes at 1530 and 1251 cm^{-1}, as well as for the characteristic rU mode at 1231 cm^{-1}. Hypochromic effect accompanied by ~4 cm^{-1} downshift should also be stressed for the Raman band at

785 cm^{-1} due to the overlap of cytosine and uracil ring breathing modes. Strong hypochromism of the 1231 cm^{-1} rU Raman band proves clearly 5′-stacking of the third uracil in CUUG tetraloop (Fig. 1), the second uracil being located in the major groove and interacts with the C-G base pairs. The looped-out orientation of the second uracil in UUCG tetraloop can also be deduced from the comparison of the Raman spectra in the region above 1650 cm^{-1}. In UUCG tetraloop an intense band is observed at 1689 cm^{-1} (assigned to the carbonyl bond stretch of uracil), which is similar to the Raman bands observed in free rU or free 5′-UMP (spectra not shown), whereas in CUUG tetraloop, a less intense Raman band is observed at this position.

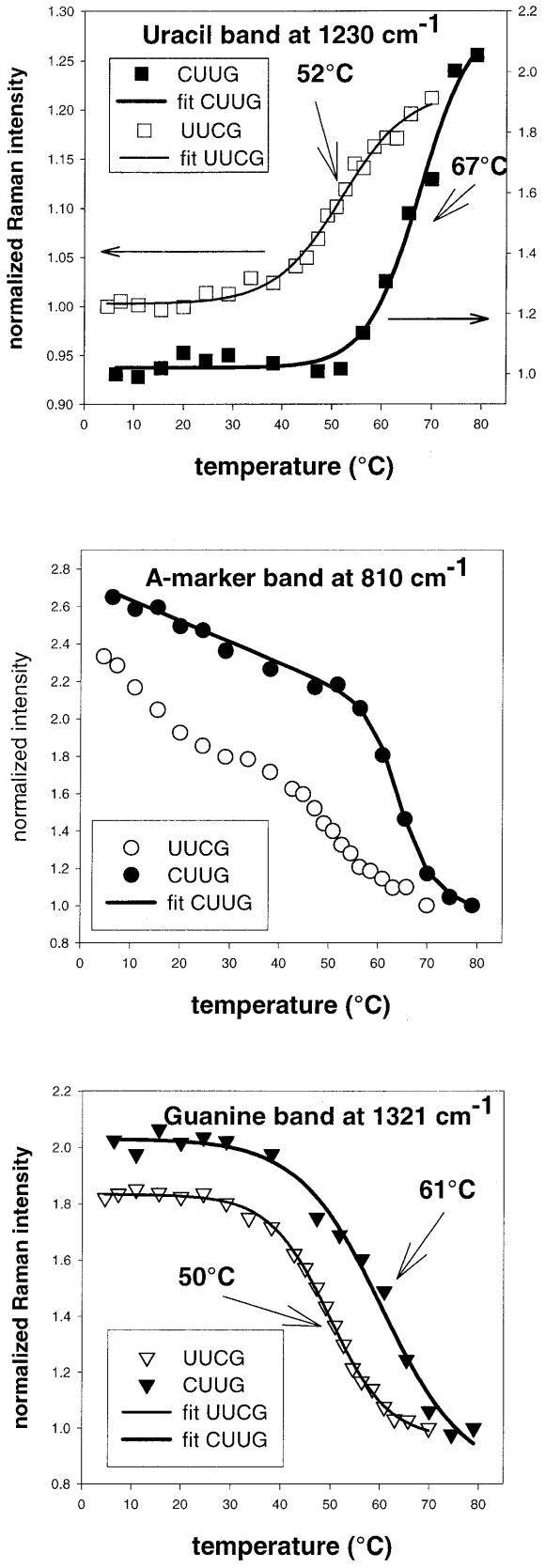

Infrared spectra can also be used to analyze the nucleotide conformations in a hairpin. In the 1250–1080 cm^{-1} region, the FT-IR spectrum recorded at room temperature (Fig. 4) shows strong bands assigned to vibrations of phosphate groups. Bands at 1221 and 1241 cm^{-1} arise from asymmetric PO_2^- stretch whereas strong complex band at 1087 cm^{-1} with partly resolved structure originates from symmetric PO_2^- stretch. The observed splitting of PO_2^- vibrations reflects differences between phosphate group environment in the stem and loop of CUUG hairpin. Both A (at 1241 and 1101 cm^{-1}) and B (at 1221 and 1087 cm^{-1}) family geometry markers (13,14) were observed. The former can be assigned to an A-form stem (double-helix with C3′-*endo* sugars) while the latter to the loop consisting only of C2′-*endo* sugars.

However, the most frequently used Raman fingerprints of an A-form helix (14) are the two Raman bands observed at 812 and 715 cm^{-1} (Fig. 3). Decrease of their intensity with increasing temperature allows us to assign them undoubtedly to an ordered structure (see negative bands in difference Raman spectra in Fig. 3). These bands confirm, in agreement with FT-IR spectra, the presence of C3′-*endo* sugar puckers in the stem of both UUCG and CUUG hairpins. It should be mentioned that the same kind of behavior has been observed in all UNCG and GNRA Raman spectra (7,18–20).

Difference Raman spectra also help us to recognize for both hairpins at low temperatures a component around 1260 cm^{-1} (Fig. 3). This component is found on the high wavenumber side of the 1251 cm^{-1} band assigned to rC. Band decomposition shown in Figure 5 clearly shows the presence of a band at 1263 cm^{-1} in Raman spectra of both UUCG (7,18) and CUUG hairpins. These two bands have been previously assigned to the rC residues in C3′-*endo/anti* (1251 cm^{-1}) and C2′-*endo/anti* (1263 cm^{-1}) conformation. This assignment has been reinforced by vibrational calculations on both rC conformers by means of *ab initio* quantum mechanical approach (27). NMR data (11) have revealed the existence of C2′-*endo/anti* rC conformers in both UUCG (located at the second and third positions) and CUUG (only located at the first position) tetraloops.

Figure 7. Temperature-dependent profiles of selected Raman bands of uracil (1231 cm^{-1}, top), guanine (1321 cm^{-1}, bottom) and phosphate-backbone (812 cm^{-1}, middle) of 5′-r(GCG-CUUG-CGC)-3′ (full symbols) and 5′-r(GC-UUCG-GC) (open symbols). Fitted curves were drawn by thick and narrow lines for the CUUG and UUCG hairpins, respectively. Temperatures indicated by arrows correspond to the inflection point of the fitted curve. Melting temperatures determined on the basis of UV absorption melting profiles are 60.7°C (this work, see Fig. 1) and 54.0°C (7) for the CUUG and UUCG hairpins, respectively.

As far as the rG Raman markers are concerned, the existence of a mode at 1313 cm^{-1} in the Raman spectra of CUUG Raman spectrum should be particularly stressed. This marker is observed as a shoulder on the low wavenumber side of the well-known rG Raman band at 1321 cm^{-1} (Fig. 5). In accordance with NMR data (10,11), we assign this new marker mode to the rG with C2′-*endo/anti* conformation found at the last position of the CUUG tetraloop.

On the other hand, the existence of a C3′-*endo/syn* rG conformer on the 3′-side of the UUCG tetraloop leads to considerable enhancement of the 1321 cm^{-1} Raman band (see the difference Raman spectra in Fig. 6). In parallel and for the same reason, intensity of the Raman band at 1421 and 1185 cm^{-1} is increased and a shoulder appears at ~640 cm^{-1}, a well-known marker for C3′-*endo/syn* rG conformer (28), on the high wavenumber side of the 632 cm^{-1} band assigned to rU and the negative band at 637 cm^{-1} is clearly seen in the difference spectrum of UUCG but not CUUG (Fig. 6B).

CONCLUSION

Like in our previous investigations (7,18–20), new results on the CUUG hairpin prove once more the suitability of vibrational spectroscopic techniques to analyze base pairing, base stacking in the loop as well as the formation of a regular double-helical stem.

It is a matter of fact that Raman spectra presented here have been obtained at an oligomer concentration several times larger than that needed for UV absorption (9 versus 0.4 mM, see sample preparation). One of the main criticisms against Raman spectroscopy (also valid for NMR spectroscopy) concerns the possibility of duplex formation at milimolar concentrations required for corresponding experiments. To clarify this point, we should first emphasize that the Raman intensity variation with increasing temperature (Fig. 3) is in agreement with the UV absorption profile (Fig. 1). In fact, non-negligible changes observed in the Raman spectra of the CUUG hairpin appear at temperatures >50°C (Fig. 3), in agreement with the UV absorption profile (Fig. 1) also showing a clear tendency of this hairpin to adopt disordered structures above 50°C. In addition, Figure 7 shows the temperature-dependent normalized Raman intensity profiles for three selected bands that present highly hypochromic vibrational modes in the CUUG and UUCG spectra, i.e. at 1231 (uracil ring planar mode), 1321 (guanine ring planar mode) and 812 cm^{-1} (phosphodiester backbone A-marker band). In both tetraloops, these intensity profiles present sigmoidal shapes but with opposite behavior: the intensity of the 1321 cm^{-1} band decreases while that of the 1231 cm^{-1} band increases with temperature. Conversely, backbone marker band at 812 cm^{-1} indicates a relatively non-cooperative structural change with a pre-melting domain ($T < T_m$) where an approximately linear decrease of intensity is observed. Similar behavior has been already reported for model DNA polynucleotides, such as poly(dA–dT)·poly(dA–dT) (23). First derivative of the fitted curves to the sigmoidal part of these profiles vanishes at temperature close to the T_m determined from UV melting profiles for both UUCG and CUUG hairpins (shown by arrows in Fig. 7).

To conclude, we should emphasize the database of Raman markers constituted by our investigations on the ultrastable tetraloops (7,18–20), for which NMR data are available in the literature, can now be used for analysis of other loops, but also other particular structures such as internal loops, bulges, etc.

ACKNOWLEDGEMENTS

V.B. would like to thank the French Ministry of National Education, Research and Technology for a PAST-PECO visiting professor fellowship. This work was partly supported by Czech Ministry of Education, Youth and Sports (project no. VS-97113).

REFERENCES

1. Uhlenbeck,O.C. (1990) Nucleic-acid structure–tetraloops and RNA folding. *Nature*, **346**, 613–614.
2. Woese,C.R., Winker,S. and Gutell,R.R. (1990) Architecture of ribosomal RNA-constraints on the sequence of tetraloops. *Proc. Natl Acad. Sci. USA*, **87**, 8467–8471.
3. Murphy,F.L. and Cech,T.R. (1994) GAAA tetraloop and conserved bulge stabilize tertiary structure of a group-I intron domain. *J. Mol. Biol.*, **236**, 49–63.
4. Varani,G., Cheong,C. and Tinoco,I.,Jr (1991) Structure of an unusually stable RNA hairpin. *Biochemistry*, **30**, 3280–3289.
5. Allain,F.H.T. and Varani,G. (1997) How accurately and precisely can RNA structure be determined by NMR? *J. Mol. Biol.*, **267**, 338–351.
6. Nowakowski,J. and Tinoco,I.,Jr (1996) Conformation of an RNA molecule that models the P4/P6 junction from group I introns. *Biochemistry*, **35**, 2577–2585.
7. Abdelkafi,M., Ghomi,M., Turpin,P.-Y., Baumruk,V., Hervé du Penhoat,C., Lampire,O., Bouchemal-Chibani,N., Goyer,P., Namane,A., Gouyette,C., Huynh-Dinh,T. and Bednarova,L. (1997) Common structural features of UUCG and UACG tetraloops in very short hairpins determined by UV absorption, Raman, IR and NMR spectroscopies. *J. Biomol. Struct. Dyn.*, **14**, 579–593.
8. Jucker,F.M., Heus,H.A., Yip,P.F., Moors,E.H.M. and Pardi,A. (1996) A network of heterogeneous hydrogen bonds in GNRA tetraloops. *J. Mol. Biol.*, **264**, 968–980.
9. Orita,M., Nishikawa,F., Shimayama,T., Taira,K., Endo,Y. and Nishikawa,S. (1993) High-resolution NMR study of a synthetic oligoribonucleotide with a tetranucleotide GAGA loop that is a substrate for the cytotoxic protein, ricin. *Nucleic Acids Res.*, **21**, 5670–5678.
10. Jucker,F.M. and Pardi,A. (1995) Solution structure of the CUUG hairpin loop—a novel RNA tetraloop motif. *Biochemistry*, **34**, 14416–14427.
11. Varani,G. (1995) Exceptionally stable nucleic acid hairpins. *Annu. Rev. Biophys. Biomol. Struct.*, **24**, 379–404.
12. Saenger,W. (1984) Defining terms for nucleic acids. In Cantor,C.R. (ed.), *Principles of Nucleic Acid Structure.* Springer-Verlag, New York, NY, pp. 14–23.
13. Thomas,G.J.,Jr and Wang,A.H.J. (1988) Laser Raman spectroscopy of nucleic acids. In Eckstein,F. and Lilley,D.M.J. (eds), *Nucleic Acids and Molecular Biology*. Springer Verlag, Berlin, Vol. **12**, pp. 1–29.
14. Peticolas,W.L. and Evertsz, E. (1992) Conformation of DNA *in vitro* and *in vivo* from laser Raman scattering. In Lilley,D.M.J. and Dahlberg,J.E. (eds), *Methods Enzymology*. Academic Press, New York, NY, Vol. **211**, Part A, pp. 334–352.
15. Small,E.W., Brown,K.G. and Peticolas,W.L. (1972) Structural changes in t-RNA from changes in the Raman scattering intensities. *Biopolymers*, **11**, 1209–1215.
16. Liquier,J. and Taillandier,E. (1996) Infrared spectroscopy of nucleic acids. In Mantsch,H.H. and Chapman,D. (eds), *Infrared Spectroscopy of Biomolecules*. Wiley Interscience, New York, NY, pp. 131–158.
17. Deng,H., Bloomfield,V.A., Benevides,J.M. and Thomas, G.J.,Jr (1999) Dependence of the Raman signature of genomic B-DNA on nucleotide base sequence. *Biopolymers*, **50**, 656–666.
18. Abdelkafi,M., Leulliot,N., Baumruk,V., Bednarova,L., Turpin,P.-Y., Namane,A., Gouyette,C., Huynh-Dinh,T. and Ghomi,M. (1998) Structural features of the UCCG and UGCG tetraloops in very short hairpins as evidenced by optical spectroscopy. *Biochemistry*, **37**, 7878–7884.

19. Leulliot,N., Baumruk,V., Abdelkafi,M., Turpin,P.-Y., Namane,A., Gouyette,C., Huynh-Dinh,T. and Ghomi,M. (1999) Unusual nucleotide conformations in GNRA and UNCG type tetraloop hairpins: evidence from Raman markers assignments. *Nucleic Acids Res.*, **27**, 1398–1404.
20. Leulliot,N., Baumruk,V., Gouyette,C., Huynh-Dinh,T., Turpin,P.-Y. and Ghomi,M. (1999) Aqueous phase structural features of GNRA tetraloops formed in short hairpins as evidenced by UV absorption and Raman spectroscopy. *Vibrational Spectrosc.*, **19**, 335–340.
21. Antao,V.P., Lai,S.Y. and Tinoco,I.,Jr (1991) A thermodynamic study of unusually stable RNA and DNA hairpins. *Nucleic Acids Res.*, **19**, 5901–5905.
22. Antao,V.P. and Tinoco,I.,Jr (1992) Thermodynamic parameters for loop formation in RNA and DNA hairpin tetraloops. *Nucleic Acids Res.*, **20**, 819–824.
23. Movileanu,L., Benevides,J.M. and Thomas,G.J.,Jr (1999) Temperature dependence of the Raman spectrum of DNA. Part I – Raman signatures of premelting and melting transitions of poly(dA-dT).poly(dA-dT). *J. Raman Spectrosc.*, **30**, 637–649.
24. Dousseau,F., Therrien,M. and Pézolet,M. (1989) On the spectral subtraction of water from the FT-IR spectra of aqueous solutions of proteins. *Appl. Spectrosc.*, **43**, 538–542.
25. Puglisi,J.D. and Tinoco,I.,Jr (1989) Absorbance melting curves of RNA. *Methods Enzymol.*, **180**, 304–325.
26. Thomas,G.J.,Jr and Tsuboi,M. (1993) Raman spectroscopy of nucleic acids and their complexes. *Adv. Biophys. Chem.*, **3**, 1–70.
27. Leulliot,N., Ghomi,M., Jobic,H., Bouloussa,O. and Baumruk,V. (1999) Ground state properties of the nucleic acid constituents studied by density functional calculations. 2. Comparison between calculated and experimental vibrational spectra of uridine and cytidine. *J. Phys. Chem. B*, **103**, 10934–10944.
28. Trulson,M.O., Cruz,P., Puglisi,J.D., Tinoco,I.Jr and Mathies,R.A. (1987) Raman spectroscopic study of left-handed Z-RNA. *Biochemistry*, **26**, 8624–8630.